

The Coldest Known Y Dwarfs: Estimates of their Effective Temperatures

S. K. LEGGETT ¹

¹*Gemini Observatory/NSF's NOIRLab, 670 N. A'ohoku Place, Hilo, HI 96720, USA*

ABSTRACT

For a decade there has been a factor of 2.5 gap in luminosity between the 275 K WISE J085510.83-071442.5 (Luhman 2014) and all other Y dwarfs, with $T_{\text{eff}} \gtrsim 350$ K. Recently three objects were found which may fall in this gap. Two are companions to Y dwarfs: WISE J033605.05-014350.4B (Calissendorff et al. 2023) and CWISEP J193518.58-154620.3B (De Furio et al. 2025); the third is MEAD 62B, a candidate companion to a white dwarf (Albert et al. 2025a). Evolutionary models calculate a tight relationship between luminosity and T_{eff} for Y dwarfs. I determine luminosities and hence T_{eff} for three Y dwarfs (WISE J085510.83-071442.5, WISE J173835.53+273259.0, WISE J182831.08+265037.7). I derive relationships between T_{eff} and mid-infrared colors using these together with 22 T and Y dwarfs from Beiler et al. (2024) with luminosity-based T_{eff} values. These relationships are used to explore the T_{eff} distribution for Y dwarfs. A sample of 31 Y dwarfs within ~ 20 pc is presented with $275 < T_{\text{eff}} < 425$ K. The *JWST* colors for WISE J053516.80-750024.9 and WISE J182831.08+265037.7 support previous suggestions that they are unresolved binaries, the former a 480 K and 340 K dwarf pair and the latter a pair of 387 K dwarfs. Five other dwarfs have unusual colors; two are likely high gravity and/or metal-poor (WISE J024714.52+372523.5, WISEA J215949.54-480855.2), two low gravity and/or metal-rich (CWISEP J104756.81+545741.6, WISE J150115.92-400418.4), and the fifth cannot be interpreted (WISE J043052.92+463331.6). An Appendix provides colors which can be used as a reference for searches for brown dwarfs in *JWST* data.

Keywords: Brown dwarfs — Exoplanet astronomy — Fundamental parameters of stars — Infrared photometry

1. INTRODUCTION

Brown dwarfs have insufficient mass for sustained energy production by nuclear fusion, and cool over periods of gigayears (e.g. Marley et al. 2021, their Figure 13). The coldest brown dwarfs are classified as Y dwarfs, and have effective temperatures (T_{eff}) less than 500 K (Cushing et al. 2011; Kirkpatrick et al. 2021a). The warmer T-type brown dwarfs have $500 \lesssim T_{\text{eff}} < 1200$ K (e.g. Kirkpatrick et al.

2021a, their Figure 22). Note that spectral type is based on the appearance of near-infrared spectra and not on T_{eff} (Burgasser et al. 2006; Cushing et al. 2011; Kirkpatrick et al. 2012).

The discovery of WISE J085510.83–071442.5 (hereafter WISE 0855-07) was presented by Luhman (2014). It is a remarkably cold brown dwarf, with a T_{eff} of only 275 K (Luhman et al. 2024; Kühnle et al. 2024; Leggett et al. 2025a); it is also very close, only 2 pc from the Sun (Luhman & Esplin 2016). It holds the record for the least luminous brown dwarf known with $\log L/L_{\odot} \approx -7.2$. Until very recently there was a large gap in luminosity between it and all other known brown dwarfs, with the next luminous brown dwarf being more than $2.5\times$ brighter, having $T_{\text{eff}} \gtrsim 350$ K and $\log L/L_{\odot} \gtrsim -6.8$.

Scientists using the *James Webb Space Telescope* (*JWST*) are now discovering objects within this temperature and luminosity gap, thanks to *JWST*'s sensitivity to mid-infrared light, and the instruments' high spatial resolution. Two of the objects that lie in the gap are close companions to other Y dwarfs, forming the tight binary systems WISE J033605.05-014350.4AB (Calissendorff et al. 2023, hereafter WISE 0336-01AB) and CWISEP J193518.58-154620.3AB (De Furio et al. 2025, hereafter WISE 1935-15AB). A third object is a candidate brown dwarf companion to the white dwarf MEAD 62 (also known as 2MASS J09424023-4637176, Albert et al. 2025a). The analyses by Albert et al. (2025a) confirm that MEAD 62B is an unresolved point source, however they estimate that there is a 50% chance that the object is a false-positive red dot. Multi-epoch observations are needed to measure a proper motion for the source, to determine whether or not it is associated with the white dwarf. The mid-infrared colors and luminosity of the source are consistent with it being a cold brown dwarf at the distance of the white dwarf.

In this work I explore the relationships between mid-infrared luminosity, color, and T_{eff} for a sample of brown dwarfs, with particular emphasis on the coldest Y dwarfs. Using a sample of brown dwarfs with T_{eff} values determined from measurements of bolometric luminosity, relationships are determined which can be used to estimate T_{eff} for other objects.

In Section 2, I calculate the luminosities and temperatures for three Y dwarf systems, and update the values for a T dwarf system. In Section 3, I use these values, together with those determined by Beiler et al. (2024) for a sample of T and Y dwarfs, to produce regression fits to color- T_{eff} datasets. Brown dwarfs which deviate from the general population are discussed. In Section 4 the population of the coldest Y dwarfs is explored. In Section 5 the physical parameters of the three binary systems with cold Y dwarf secondaries are described. My conclusions are given in Section 6. The Appendix presents a reference set of *JWST* colors which are useful for deep searches for cold brown dwarfs in *JWST* data, such as the JADES and CEERS surveys (Hainline et al. 2024, 2025).

2. LUMINOSITIES AND EFFECTIVE TEMPERATURES FOR Y DWARFS

The theory of how brown dwarfs evolve, in terms of their mass, radius and luminosity, is well established (e.g. Burrows & Liebert 1993; Burrows et al. 1997). Comparison of the evolutionary models to measurements of radius and mass for brown dwarfs and giant planets shows good agreement (Marley et al. 2021). Figure 1 is a luminosity: T_{eff} plot, with data taken from the evolutionary models of Marley et al. (2021). Isochrones are shown for ages of 0.5 Gyr and 10 Gyr; these ages span the likely range in age for a local sample of brown dwarfs (e.g. Buder et al. 2019), although the population synthesis of brown dwarfs within 25 pc by Best et al. (2024) shows that more than 90% of the population is younger than 4 Gyr. As luminosity decreases the range in T_{eff} becomes small, so

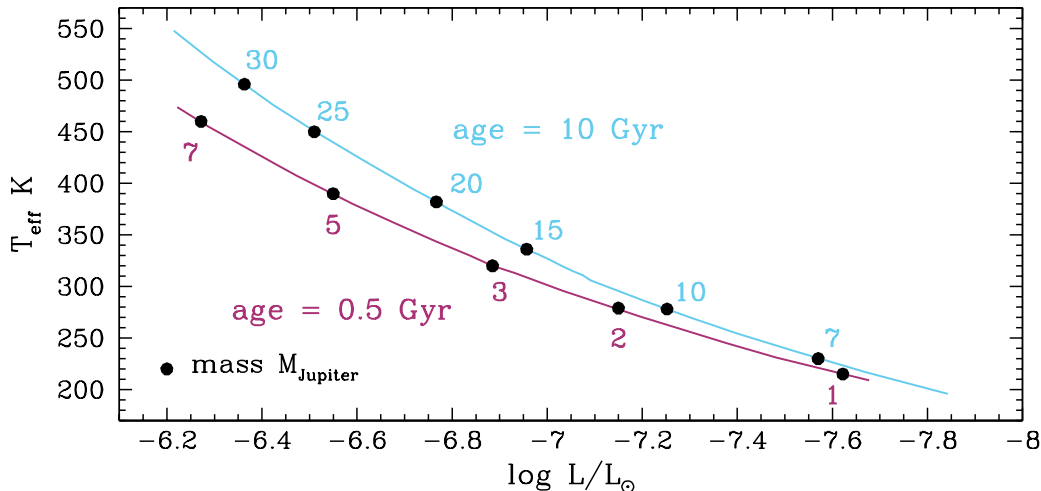


Figure 1. Relationship between effective temperature and luminosity for solar-metallicity brown dwarfs, from the evolutionary models by Marley et al. (2021). The upper blue line is for older brown dwarfs with an age of 10 Gyr, and the lower red line is for younger brown dwarfs with an age of 0.5 Gyr. Dots along the sequences indicate mass in units of M_{Jupiter} .

that luminosity significantly constrains T_{eff} for cold brown dwarfs. Note that mass is not constrained by luminosity — in order to estimate mass a measurement of surface gravity is required (see Marley et al. 2021, their Figure 10).

In this work I use a sample of brown dwarfs that have published spectra covering a broad range of wavelength including the mid-infrared, where most of the energy is emitted by cold objects. With these data, a reliable determination of bolometric luminosity can be made, constraining T_{eff} (Figure 1). The Beiler et al. (2024) sample is the primary data source; low-resolution NIRSPEC and MIRI spectra were obtained for twenty-two T and Y dwarfs covering the wavelength range $0.8 \leq \lambda \mu\text{m} \leq 12.0$. Longer wavelength photometry was also obtained using MIRI with the F1000W, F1500W, F1800W and F2100W filters. Beiler et al. (2024) extended the spectral energy distribution (SED) beyond $21 \mu\text{m}$ by adopting a Rayleigh–Jeans flux distribution. For one of the T dwarfs in the Beiler et al. (2024) sample, SDSSp J134646.45-003150.4, Vrba et al. (2026) determined a parallax that is more precise and significantly different from the value used by Beiler et al. (2024). I have used the newer parallax to revise the luminosity and T_{eff} for this object, and the values are given in Table 1. The brown dwarf is $\approx 10\%$ closer, making the luminosity $\approx 20\%$ fainter, and $T_{\text{eff}} \approx 5\%$ lower.

I have added three Y dwarfs to the luminosity sample, which all have published MIRI spectra:

- WISE 0855-07 — *JWST* NIRSPEC spectra covering $0.8 \leq \lambda \mu\text{m} \leq 5.5$ was published by Luhman et al. (2024). *JWST* MIRI spectra covering $5.2 \leq \lambda \mu\text{m} \leq 22$ was published by Kühnle et al. (2024). I extended the SED beyond $22 \mu\text{m}$ by adopting a Rayleigh–Jeans flux distribution. The observed portion of the bolometric flux makes up 84% of the total, with the Rayleigh–Jeans extension making up 16%. For the observational fraction of the SED, I assume that the un-

Table 1. Luminosity and Implied T_{eff} for an Age Range of 0.5 to 10 Gyr

Name	Distance*	F_{bol}	L_{bol}	$\log L/L_{\odot}$	T_{eff}
	pc	$10^{-16} \text{ W m}^{-2}$	10^{20} W		K
WISE J085510.83-071442.5	2.28 ± 0.01	3.71 ± 0.15	0.230 ± 0.009	-7.22 ± 0.02	276 ± 9
SDSSp J134646.45-003150.4**	$13.20^{+0.22}_{-0.06}$	11.26 ± 0.16	23.5 ± 1.6	-5.21 ± 0.03	927^{+58}_{-87}
WISE J173835.53+273259.0	7.64 ± 0.12	1.77 ± 0.14	1.24 ± 0.15	-6.49 ± 0.05	431 ± 27
WISE J182831.08+265037.7	9.97 ± 0.19	1.39 ± 0.04	1.65 ± 0.04	-6.37 ± 0.02	$387 \pm 22^{***}$

*Distances are determined from parallaxes published in Kirkpatrick et al. (2021a), except for SDSSp J134646.45-003150.4 for which the parallax published by Vrba et al. (2026) is used.

** The luminosity and T_{eff} have been revised from the values determined by Beiler et al. (2024) using the parallax published by Vrba et al. (2026). The uncertainty in T_{eff} has been set to that quoted by Beiler et al. (2024).

***The T_{eff} is determined assuming WISE J182831.08+265037.7 consists of an identical pair of Y dwarfs. If this object is single then the luminosity implies $T_{\text{eff}} = 462 \pm 25$.

certainty equals the uncertainty in the absolute flux calibration of the instruments, which is currently estimated to be 3%. Estimating an uncertainty of 10% for the Rayleigh–Jeans tail (based on the uncertainty of defining a “continuum” point at which to start the extension), the total uncertainty in the bolometric flux is 4%. I adopt a range for T_{eff} assuming a possible range in age of 0.5 Gyr to 10 Gyr. The results are given in Table 1.

- WISE J173835.53+273259.0 (hereafter WISE 1738+27) — near-infrared ground-based spectra covering $1.0 \leq \lambda \mu\text{m} \leq 2.2$ was published by Cushing et al. (2011) and Leggett et al. (2016). *JWST* MIRI spectra covering $4.9 \leq \lambda \mu\text{m} \leq 18$ was published by Vasist et al. (2025). I use ATMO 2020++ without PH_3 synthetic spectra (Phillips et al. 2020; Leggett et al. 2021; Meisner et al. 2023; Leggett & Tremblin 2025) to bridge the $2.2 \leq \lambda \mu\text{m} \leq 4.9$ gap, selecting spectra from the available grids which reproduce the observed spectra and the *WISE* W2 and *JWST* F480M photometry measured for this dwarf (ALLWISE Catalog and Albert et al. 2025b). A $T_{\text{eff}} = 400 \text{ K}$, $\log g = 4.0$ solar metallicity synthetic spectrum reproduces the data well. This spectrum was also used to extend the SED to $\lambda = 30 \mu\text{m}$ (where the model terminates), beyond which a Rayleigh–Jeans tail was adopted. For this object, the observed portion of the SED makes up 63% of the total flux, the modelled $2.2 \leq \lambda \mu\text{m} \leq 4.9$ region around 24%, and the region at $\lambda > 18 \mu\text{m}$ 13%. By exploring variations in the the model fluxes around the critical $\lambda \sim 4.5 \mu\text{m}$ region, I estimate an uncertainty in the total bolometric flux of 8%. Again a range in age of 0.5 Gyr to 10 Gyr is adopted, and T_{eff} values determined accordingly. The results are given in Table 1.
- WISE J182831.08+265037.7 (hereafter WISE 1828+26) — *JWST* NIRSpec low-resolution spectra covering $0.8 \leq \lambda \mu\text{m} \leq 5.3$ was obtained as part of the *JWST* Cycle 1 GTO program 1189, PI: Thomas Roellig. Higher resolution NIRSpec spectra overing $2.9 \leq \lambda \mu\text{m} \leq 5.1$ was published by Lew et al. (2024). *JWST* MIRI spectra covering $4.9 \leq \lambda \mu\text{m} \leq 18$ was published by Barrado et al. (2023). This object has been recognized to be significantly super-luminous, but

has not been resolved into a multiple system in high spatial resolution imaging (e.g. [Beichman et al. 2013](#); [De Furio et al. 2023](#)). Here I adopt the solution found by [Leggett & Tremblin \(2025\)](#) in an exploratory fit of ATMO 2020++ grid spectra to the *JWST* data: that the system is a pair of similar cold brown dwarfs with T_{eff} between 350 K and 400 K, surface gravities g in the range $\log g$ 4.5 to 5.0 dex, with solar or slightly subsolar metallicity. In order to complete the SED for this work, I used two $T_{\text{eff}} = 400$ K, $\log g = 5.0$ solar metallicity synthetic spectra to extend the MIRI observations from $18 \mu\text{m}$ to $30 \mu\text{m}$, beyond which a Rayleigh–Jeans tail was adopted. For this object, the observed portion of the SED makes up 91% of the total, with the model and Rayleigh–Jeans extension making up 9%. The uncertainty in the bolometric flux is dominated by the uncertainty in the [absolute flux calibration of the instruments, which is currently estimated to be 3%](#). Again a likely range in age of 0.5 Gyr to 10 Gyr is adopted, and T_{eff} values determined accordingly. The results are given in Table 1.

3. COLOR AND T_{EFF} FOR BROWN DWARFS

3.1. Dataset

In this Section I use the luminosity-based T_{eff} values for the twenty two T and Y dwarfs from the [Beiler et al. \(2024\)](#) sample, together with the three additional Y dwarfs described above, to determine relationships between various colors and T_{eff} . The sample is representative of the local field population, but does not include more extreme objects like subdwarfs — [Beiler et al. \(2024\)](#) chose targets with a range in color at a given $\lambda \approx 5 \mu\text{m}$ luminosity ([Beiler et al. 2024](#), their Figure 1), but excluded dwarfs suspected to be extremely metal-poor.

Figures 2 through 4 show T_{eff} as a function of various colors, for the sample of 25 T and Y dwarfs. I show the relationships for $J - W2$, $J - [4.5]$, and $[3.6] - [4.5]$ in Figure 2; these are commonly available and frequently used colors for brown dwarfs. Figure 3 shows the relationships for absolute magnitudes at $\lambda \sim 4.5 \mu\text{m}$, where there is a peak in the SED (see e.g. [Beiler et al. 2024](#), their Figures 5 – 7). The absolute W2 and [4.5] magnitudes are shown, as well as magnitudes for two *JWST* filters that have been used in studies of brown dwarfs, F444W and F480M. F444W and F480M magnitudes were synthesized by [Beiler et al. \(2024\)](#) from their data, and I use those values here. For WISE 0855-07, WISE 1738+27, and WISE 1828+26, the F480M magnitudes are taken from [Albert et al. \(2025b\)](#). F444W magnitudes were synthesized for WISE 0855-07 and WISE 1828+26 from the NIRSspec data published by [Luhman et al. \(2024\)](#) and [Lew et al. \(2024\)](#). Figure 4 shows the relationships for three longer wavelength *JWST* filters: F1000W, F1500W, and F1800W. For WISE 0855-07, WISE 1738+27, and WISE 1828+26, these magnitudes were synthesized from the MIRI spectra published by [Kühnle et al. \(2024\)](#); [Vasist et al. \(2025\)](#); [Barrado et al. \(2023\)](#). The data only span the F1800W filter for WISE 0855-07. Table 2 gives the values of the magnitudes synthesized here.

I do not include the [Beiler et al. \(2024\)](#) F2100W results because [MIRI’s sensitivity](#) decreases rapidly at wavelengths longer than $18 \mu\text{m}$ and the F2100W filter is unlikely to be used for cold brown dwarf science. Also, although some brown dwarf data have been taken using the F1280W filter, the [Beiler et al. \(2024\)](#) spectra do not extend to wavelengths long enough to span the filter bandpass, and so it cannot be synthesized and included in this work.

Table 2. Synthesized Photometry, Vega Magnitudes

Name	F444W	F1000W	F1500W	F1800W
WISE J085510.83-071442.5	14.08	12.12	10.40	10.02
WISE J173835.53+273259.0	...	12.66	11.71	...
WISE J182831.08+265037.7	14.45	13.11	12.02	...

NOTE—The uncertainty is dominated by the uncertainty in the absolute flux calibration of the *JWST* instruments, which is currently estimated to be 3% or 0.03 magnitudes.

3.2. Weighted Regression Fits

The initial sample for determining a relationship between T_{eff} and color consisted of 25 T and Y dwarfs. Figures 2, 3 and 4 show that there are some obvious outliers in the sequences. I removed six sources which deviated from the fits by 3σ or more. These sources were removed from all fits, including those colors where they did not appear to deviate, in order to have a sample 19 dwarfs with consistent T_{eff} across all colors used here. (For F444W the sample size is 18, and for F1800W it is 17, because of the incomplete wavelength coverage for synthesizing the F444W and F1800W magnitudes (Table 2).) Non-linear regression fitting was performed, weighting the T_{eff} values by the uncertainties provided by Beiler et al. (2024) and Table 1. Cubic polynomials produced fits with an *rms* dispersion of 1.2σ or less, except at F1500W where the *rms* is 1.3σ and F1800W where it is

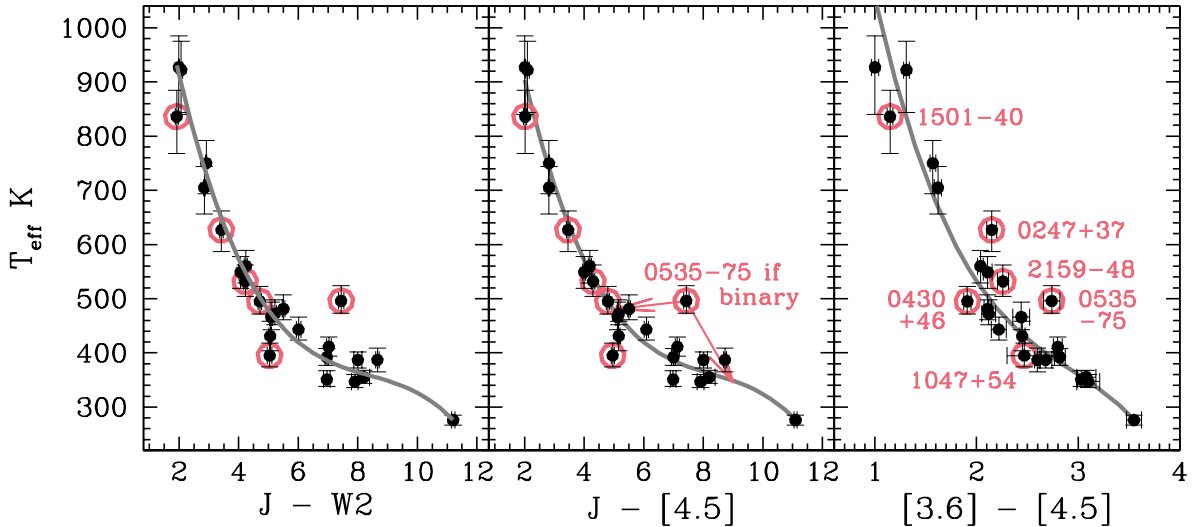


Figure 2. Luminosity-based T_{eff} for the sample of 25 T and Y dwarfs described in Section 2, as a function of $J - W2$, $J - [4.5]$, and $[3.6] - [4.5]$. Points circled in red are removed from the regression fits, the results of which are shown as thick gray lines. Parameters for the fits are given in Table 3. The six brown dwarfs omitted from the fits are identified in the right panel by an abbreviated RA and Decl. WISE 0535-75 may be a binary, composed of a 480 K and 340 K dwarf, as indicated in the middle panel.

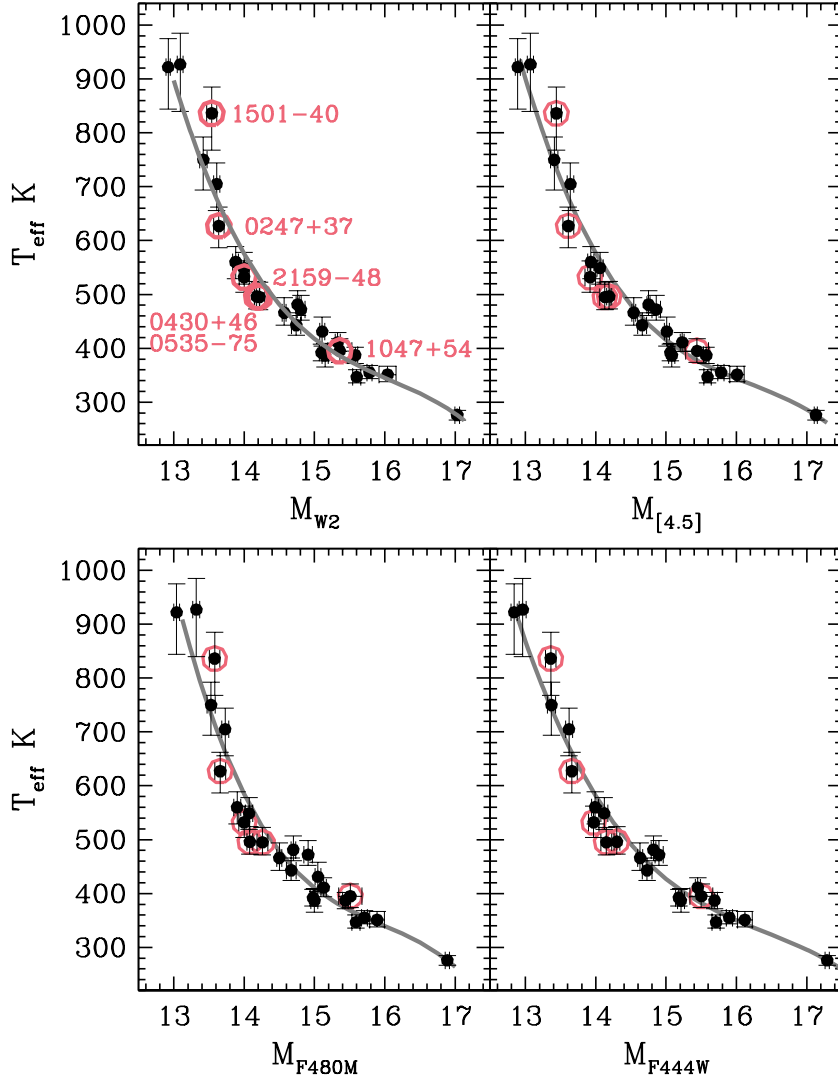


Figure 3. Luminosity-based T_{eff} for the sample of 25 T and Y dwarfs described in Section 2, as a function of absolute magnitudes at $\lambda \approx 4.5 \mu\text{m}$. Six brown dwarfs are omitted from the regression fits, identified in the top left panel, and these points are circled in red. The results of the fits are shown as gray lines and the parameters are given in Table 3.

1.8σ . Increasing the number of parameters for the fits did not significantly improve the *rms*. Table 3 gives the parameters for these fits.

For late-T and Y dwarfs, absolute magnitudes at $\lambda \sim 4.5 \mu\text{m}$ can provide a good estimate of T_{eff} (e.g. Leggett & Tremblin 2025; Leggett et al. 2025a), while colors such as $J - [4.5]$ and $[3.6] - [4.5]$ are more sensitive to metallicity and gravity (e.g. Meisner et al. 2020a; Leggett & Tremblin 2025; Leggett et al. 2025a). Table 3 gives the dispersion in the fits shown in Figures 2, 3, and 4. The largest dispersion is for M_{F1800W} , followed by the J -band colors. All dispersions are low, however

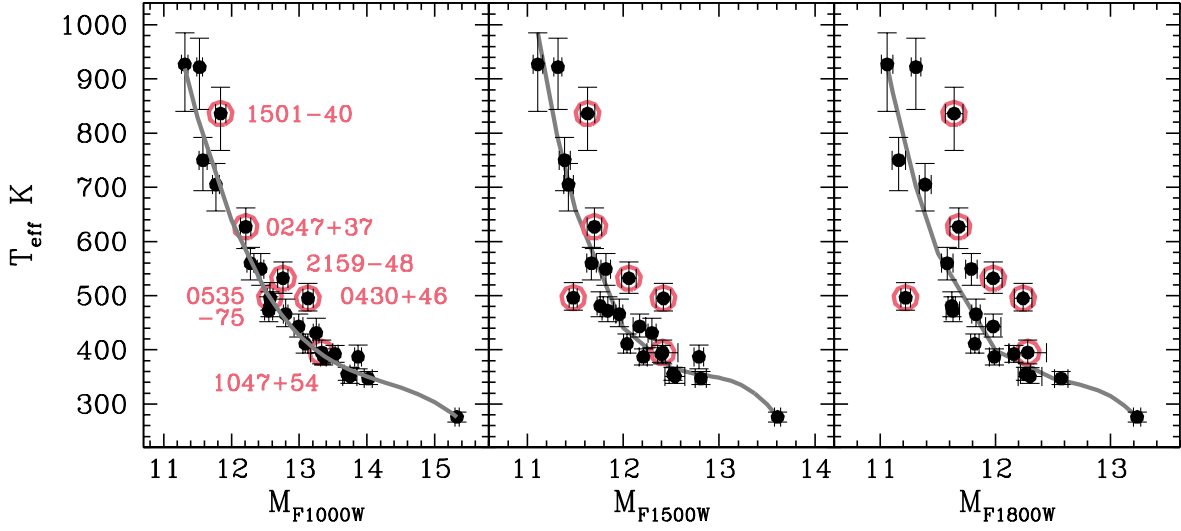


Figure 4. Luminosity-based T_{eff} for the sample of 25 T and Y dwarfs described in Section 2, as a function of absolute magnitudes at $\lambda \approx 10, 15$ and $18 \mu\text{m}$. Six brown dwarfs are omitted from the regression fits, identified left panel, and these points are circled in red. The results of the fits are shown as gray lines and the parameters are given in Table 3.

Table 3. Coefficients of Fits to Color: T_{eff} Relationships

Color, x	a_0	a_1	a_2	a_3	rms (K)	Valid for
$J - W2$	1516.78	-383.075	43.7989	-1.73969	16	$1.99 \leq J - W2 \leq 11.20$
$J - [4.5]$	1507.82	-381.645	43.9661	-1.76383	16	$2.01 \leq J - [4.5] \leq 11.10$
$[3.6] - [4.5]$	2302.47	-1735.962	550.974	-62.7196	13	$1.00 \leq [3.6] - [4.5] \leq 3.55$
M_{W2}	56119.60	-10298.389	637.2170	-13.21476	13	$12.92 \leq M_{W2} \leq 17.03$
$M_{[4.5]}$	54076.96	-9857.745	605.8006	-12.47410	13	$12.89 \leq M_{[4.5]} \leq 17.13$
M_{F480M}	74390.62	-13814.799	862.5367	-18.02330	13	$13.04 \leq M_{F480M} \leq 16.89$
M_{F444W}	42005.61	-7520.306	455.4078	-9.25657	12	$12.73 \leq M_{F444W} \leq 17.29$
M_{F1000W}	52562.93	-10898.188	760.8665	-17.77239	10	$11.31 \leq M_{F1000W} \leq 15.33$
M_{F1500W}	246853.60	-57618.770	4491.4848	-116.76018	14	$11.11 \leq M_{F1500W} \leq 13.61$
M_{F1800W}	286936.96	-68205.344	5414.2448	-143.35935	19	$11.06 \leq M_{F1800W} \leq 13.23$

NOTE— Coefficients are applied as

$$T_{\text{eff}} = a_0 + a_1 \times x + a_2 \times x^2 + a_3 \times x^3$$

*The rms of each fit is given in the Table. The total uncertainty in T_{eff} determined from these relationships is estimated to range from 20 K to 60 K for the colder to warmer brown dwarfs; see Section 3.2.

this is for a small sample of typical field age and metallicity brown dwarfs. Applying the J – W2, J – [4.5], [3.6] – [4.5], M_{W2} , and $M_{[4.5]}$ relationships, or a subset, to a photometric data set of 308 dwarfs cooler than 1000 K, produced standard deviations (s) in T_{eff} which increased with T_{eff} . This reflects the increasing steepness of the color: T_{eff} curve with increasing T_{eff} (Figures 2, 3, and 4). After 3σ -clipping, for $T_{\text{eff}} \approx 350$ K, $s = 20$ K; for $T_{\text{eff}} \approx 550$ K, $s = 41$ K; and for $T_{\text{eff}} \approx 750$ K, $s = 57$ K. These values, of $\approx 7\%$ in T_{eff} , represent the uncertainty floor when using the relationships in Table 3. Extreme outliers in metallicity or gravity can have an even larger dispersion in T_{eff} across the colors, as shown in the Section 3.3.

3.3. Atypical Brown Dwarfs

The six sources excluded from the regression fits, and circled in red in Figures 2, 3, and 4, are:

- WISE J024714.52+372523.5: red in [3.6] – [4.5] and the spectrum shows weak CO₂ and CO for a T8 dwarf (Figure 4 of Tu et al. 2024). This object may be metal-poor or have a high gravity (Tu et al. 2024; Leggett & Tremblin 2025).
- WISE J043052.92+463331.6: appears faint at long wavelengths (Figure 4) and bright at $\lambda \approx 4.5$ μm compared to other T8 dwarfs (Beiler et al. 2024; Tu et al. 2024). It has the bluest F444W – F1000W color in the Beiler et al. (2024) sample, and has been flagged as abnormally red in H – W2 and faint in H by Best et al. (2021). Beiler et al. (2024) and Tu et al. (2024) also flag this brown dwarf as peculiar in their analyses of the *JWST* data. It is currently unclear what could produce such an SED.
- WISE J053516.80–750024.9 (hereafter WISE 0535-75): has extremely weak CO₂ and CO absorption (Beiler et al. 2024; Tu et al. 2024), leading to very red J – W2, J – [4.5], and [3.6] – [4.5] colors. This object may be very metal-poor and/or have a high gravity, or it may be a binary system. In a preliminary comparison of the *JWST* spectra to ATMO 2020++ synthetic spectra, Leggett & Tremblin (2024) found that reasonable fits could be obtained with a $T_{\text{eff}} = 500$ K, $\log g = 4.5$, $[\text{m}/\text{H}] = -0.5$ synthetic spectrum. A slightly better fit was obtained adopting a binary solution of 450 K and 350 K solar-metallicity brown dwarfs. Using the color relationships determined here, I find that the J – [4.5] and [3.6] – [4.5] colors, and the absolute [4.5], F1000W, F1500W, and F1800W magnitudes, are well reproduced if the system is a binary composed of a 480 K and 340 K Y dwarf pair. This is illustrated in Figure 2 for the J – [4.5] color.
- CWISEP J104756.81+545741.6 (hereafter WISE 1047+54): blue J – W2 and J – [4.5], with strong CO₂ and CO (Figure 4 of Tu et al. 2024). This object is very likely to be a young, metal-rich, low-gravity and low-mass dwarf (Beiler et al. 2024; Leggett et al. 2025a).
- WISE J150115.92–400418.4: sub-luminous at $\lambda \approx 4.5$ μm , with strong CO₂ and CO (Figure 4 of Tu et al. 2024). This T dwarf is likely to be metal-rich or have a low gravity.
- WISEA J215949.54-480855.2: red in [3.6] – [4.5] and the spectrum shows weak CO₂ and CO for a T9 dwarf (Figure 4 of Tu et al. 2024). This object may be metal-poor or have a high gravity; the relatively high tangential velocity of 82 km s^{–1} (Kirkpatrick et al. 2021a) may support membership of an older disk population (Dupuy & Liu 2012, their Figure 31).

4. THE COOLEST Y DWARFS

Table 4 includes all cold solar neighborhood Y dwarfs from the literature that the author is aware of (as of February 2026), with $T_{\text{eff}} < 425$ K. Luminosity-based T_{eff} values are given, where they exist. T_{eff} values are also given for available colors using the relationships of Table 3. The uncertainties in the color values are the square root of the sum of the squares of the *rms* for the relationship (Table 3) and the δT_{eff} due to the uncertainty in the color. The photometry is taken from Table 2 and Leggett et al. (2025b).

The adopted T_{eff} values in Table 4 are equal to the luminosity-based values where available. Otherwise the adopted T_{eff} values are the weighted mean of the color values, where I have first averaged the results from $J-W2$ and $J-[4.5]$, and the results from M_{W2} , $M_{[4.5]}$, and M_{F480M} , as these sample the same region of the SED. The quoted uncertainty in the color-based T_{eff} values is the uncertainty in the weighted mean or 20 K, whichever is larger (see Section 3.2). The color-based T_{eff} values are within 2σ of the adopted values except for WISE 1047+54, previously discussed and thought to be unusually low-gravity and metal-rich. For CWISEP J225628.97+400227.3 the T_{eff} values determined from $J-W2$ and $J-[4.5]$ are 70 K higher than the values determined from $[3.6]-[4.5]$, M_{W2} , and $M_{[4.5]}$ and I exclude them from the mean; this object is faint at J and it is possible that the uncertainty in the J measurement by Meisner et al. (2020a), although already large, has been underestimated.

Three of the Y dwarfs do not have a measured parallax: WISE J021243.55+053147.2, WISE J125721.01+715349.3, and WISE J235120.62-700025.8. A photometric distance is given in Table 4 in square brackets based on the the observed $\lambda \sim 5 \mu\text{m}$ magnitudes and the absolute magnitude indicated by the T_{eff} value. The uncertainty in the photometric distance due to the scatter in the T_{eff} -color relationships is $\approx 10\%$. A photometric distance is also given for WISE J223022.60+254907.5 which has a very uncertain parallax.

The distant candidate Y dwarfs identified in the JADES survey (Hainline et al. 2024) are not included in Table 4. Hainline et al. (2025, their Table 6) lists three candidates cooler than 400 K, with $325 \lesssim T_{\text{eff}} \lesssim 380$: JADES-GS-BD-5 at a distance of ~ 80 pc, JADES-GS-BD-21 at a distance of ~ 800 pc, and JADES-GN-BD-16 at a distance of ~ 900 pc. Hainline et al. (2025) uses various *JWST* color criteria to select candidate Y dwarfs. In the Appendix I explore these colors further.

Table 4. Candidate Brown Dwarfs with $T_{\text{eff}} < 425$ K

WISE J or Other Name	Distance pc	Lumin.	T_{eff} (K)							Adopted	Ref.
			$J-W2$	$J-[4.5]$	$[3.6]-[4.5]$	M_{W2}	$M_{[4.5]}$	M_{F480M}	M_{F1000W}		
014656.66 +423410.0B	19.34±0.72			429±16	408±16		436±25		373±20	411±20	1,2,18, 26
021243.55 +053147.2	[13.0±1.3]		394±16	394±16	372±32					391±20	3,26
033605.05 -014350.4B	10.02±0.22							308±26		308±26	4,5,18, 22
035000.32 -565830.2	5.67±0.07		376±16	377±16	327±17	349±13	349±13			355±20	1,18,27
040235.55	$8.6^{+1.8}_{-1.3}$		358±18	356±18	395±22	350±29	356±28			364±20	3,19,26

Table 4 continued on next page

Table 4 (continued)

WISE J or Other Name	Distance pc	T_{eff} (K)									Adopted	Ref.	
		Lumin.	$J - W2$	$J - [4.5]$	$[3.6] - [4.5]$	M_{W2}	$M_{[4.5]}$	M_{F480M}	M_{F1000W}	M_{F1500W}			
-265145.4													
041022.71	6.54±0.03		455±16	460±16	431±13	416±13	407±13	420±14	405±11	388±13	420±20	6,20,28	
+150248.4												29	
050305.68	10.2±0.4		398±16	400±16	362±25	348±15	345±14				364±20	7,19,26	
-564834.0													
053516.80	14.56±0.43										340±20*	1,19,30	
-750024.9B													
064723.23	10.05±0.17		367±16	368±16	382±16	408±14	410±14	421±15			394±20	8,19,18,	
-623235.5												26,27,31	
WD 0806-661B	19.23±0.01		353±16	355±16	426±15	392±17	383±16				383±20	9,21,27,31	
082507.35	6.55±0.09	387±15	365±16	365±16	400±14	370±13	369±13	373±14	390±11	397±17	387±15	10,19,18,	
+280548.5												30	
083011.95	10.08 ^{+0.71} _{-0.62}				326±22	346±18	354±16	362±17			345±20	11,22,26	
+283716.0													
085510.83	2.28±0.01	276±9	276±15	276±16	277±16	276±14	276±13	276±14	276±10	276±17	276±9	12,18,30	
-071442.5													
094005.50	15.06 ^{+3.39} _{-2.33}		421±16	414±16	388±23	416±49	431±53				413±20	3,19,26	
+523359.2													
MEAD 62B**	20.48±0.01								294±11	312±15	299±20	13,23	
104756.81	14.7 ^{+1.1} _{-1.0}	395 ⁺²³ ₋₂₁	476±16	481±16	431±28	387±21	378±19	368±18	393±20	374±23	395 ⁺²³ ₋₂₁	3,24,30	
+545741.6													
125721.01	[14.0±1.4]		378±16	381±16	394±23						382±20	7,26	
+715349.3													
140518.40	6.32±0.10	392 ⁺¹⁶ ₋₁₅	386±16	386±16	382±14	408±14	410±14	413±15	395±11	374±15	392 ⁺¹⁶ ₋₁₅	6,19,3,	
+553421.4												28,29	
144606.62	9.63 ^{+0.49} _{-0.44}	351 ⁺¹⁶ ₋₁₃	386±16	386±16	357±13	343±16	344±14	346±15	363±12	364±16	351 ⁺¹⁶ ₋₁₃	3,24,26,	
-231717.8												30	
154151.66	6.02±0.04	411 ⁺¹⁸ ₋₁₇	384±15	383±16	385±13	388±14	394±13	393±13	415±11	429±19	411 ⁺¹⁸ ₋₁₇	6,18,28,	
-225025.2												30	
163940.86	4.74±0.01		389±16	389±16	411±13	395±13	396±13	400±14			398±20	14,25,18,	
-684744.6												31	
182831.08	9.97±0.19	387±22	354±16	353±16	411±13	403±14	408±14	411±15	357±11	355±14	387±22***	6,19,18,	
+265037.7A,B												30	
193054.55	9.4±0.4		380±16	379±16	338±17	377±16	382±16				372±20	7,19,26	
-205949.4													
193518.58	14.4±0.8								404±18		404±20	15,16,19	
-154620.3A													
193518.58	14.4±0.8								325 ⁺¹⁶ ₋₃₄		325 ⁺²⁰ ₋₃₄	15,16,19	
-154620.3B													
220905.73	6.18±0.08	355 ⁺¹³ ₋₁₁	361±16	362±16	350±15	358±13	356±13	356±14	365±11	365±14	355 ⁺¹³ ₋₁₁	17,19,18,	
+271143.9												31	
223022.60	14 ⁺⁴ ₋₃ [15.0±1.5]		391±16	394±17	381±36	376±45	370±39				389±20	3,19,26	
+254907.5													
225628.97	9.8 ^{+1.2} _{-1.0}		(427±24)	(425±25)	359±30	351±21	352±19				353±20	3,19	

Table 4 continued on next page

Table 4 (continued)

WISE J or Other Name	Distance pc	T_{eff} (K)										Ref.	
		Lumin.	$J - W2$	$J - [4.5]$	$[3.6] - [4.5]$	M_{W2}	$M_{[4.5]}$	M_{F480M}	M_{F1000W}	M_{F1500W}	Adopted		
+400227.3													
235120.62	[9.0±0.9]		390±17	393±17	396±18							393±20	7,32
-700025.8													
235402.79	7.66±0.20	347 ⁺¹³ ₋₁₁	366±16	367±16	347±17	369±14	368±14	363±14	350±11	354±14	347 ⁺¹³ ₋₁₁		10,19,18,
+024014.1													30

* Assuming that this super-luminous object is a binary with component T_{eff} values of 480 K and 340 K, as deconvolved with the photometry in Section 3.

** Unconfirmed companion to 2MASS J09424023-46371 (Albert et al. 2025a).

*** Assuming that this super-luminous object is composed of an identical pair of Y dwarfs (e.g Leggett & Tremblin 2025).

References—DISCOVERY: 1 – Kirkpatrick et al. (2012); 2 – Dupuy et al. (2015); 3 – Meisner et al. (2020a); 4 – Mace et al. (2013); 5 – Calissendorff et al. (2023) 6 – Cushing et al. (2011); 7 – Meisner et al. (2020b); 8 – Kirkpatrick et al. (2013); 9 – Luhman et al. (2011, aka WISE J080714.68-661848.7); 10 – Schneider et al. (2015); 11 – Bardalez Gagliuffi et al. (2020); 12 – Luhman (2014); 13 – Albert et al. (2025a, aka 2MASS J09424023-4637176B); 14 – Tinney et al. (2012); 15 – Marocco et al. (2019); 16 – De Furio et al. (2025); 17 – Cushing et al. (2014). PARALLAX: 18 – Kirkpatrick et al. (2019); 19 – Kirkpatrick et al. (2021a); 20 – Fontanive et al. (2025) 21 – Subasavage et al. (2009); 22 – Albert et al. (2025b); 23 – Gaia Collaboration et al. (2018); 24 – Beiler et al. (2024); 25 – Fontanive et al. (2021). PHOTOMETRY: 2 – Dupuy et al. (2015); 3 – Meisner et al. (2020a); 7 – Meisner et al. (2020b); 13 – Albert et al. (2025a, aka 2MASS J09424023-4637176B); 18 – Kirkpatrick et al. (2019); 22 – Albert et al. (2025b); 26 – Leggett et al. (2021); 27 – Leggett et al. (2015); 28 – Leggett et al. (2013); 29 – Leggett et al. (2019); 30 – Leggett et al. (2025a); 31 – Leggett et al. (2017); 32 – Kirkpatrick et al. (2024).

Figure 5 shows the cold Y dwarfs listed in Table 4 in a T_{eff} :distance plot and in a histogram as a function of T_{eff} . There are 31 known objects with $T_{\text{eff}} < 425$ K if WISE 0535-75 and WISE 1828+26 are unresolved binary systems, and if MEAD 62B is proven to be a Y dwarf companion to the white dwarf MEAD 62. Note that WISE 0336-01A is not included in Table 4 or Figure 5; Calissendorff et al. (2023) estimate $T_{\text{eff}} = 415 \pm 20$ K for WISE 0336-01A however using the relationships presented here I find a warmer value for this brown dwarf of $T_{\text{eff}} = 446 \pm 20$ K.

The total number with $275 < T_{\text{eff}} < 425$ K within 10 pc (which is more likely to be complete than the ~ 20 pc sample) is 20, or 18 if WISE 1828+26 is a single, warmer, brown dwarf. This translates into a number density of between $4 \times 10^{-3} \text{pc}^{-3}$ and $6 \times 10^{-3} \text{pc}^{-3}$ for Y dwarfs across the 150 K range $275 < T_{\text{eff}} < 425$, consistent with the accounting of nearby objects by Kirkpatrick et al. (2024, their Table 17). The coldest bin, with the least luminous objects, may be incomplete. Simulations by Kirkpatrick et al. (2024) assuming a constant star formation rate with low-mass cut-offs of 1, 5, or 10 M_{Jupiter} , imply that the number of objects with $150 < T_{\text{eff}} < 300$ K ranges from $\approx 0.2 \times 10^{-3} \text{pc}^{-3}$ using Saumon & Marley (2008) evolutionary models, to $\approx 8 \times 10^{-3} \text{pc}^{-3}$ using Baraffe et al. (2003) models combined with a low-mass cut-off of 1 M_{Jupiter} . If the former number density is valid, then we may not find any other Y dwarfs like WISE 0855-07 within 10 pc of the Sun.

5. THE COLD BINARY SYSTEMS

Figure 6 shows evolutionary sequences for T dwarfs in the form of a T_{eff} : $\log g$ diagram. The evolutionary model is from Marley et al. (2021). Blue regions indicate the locations of the WISE 0336-01 components, and red regions the WISE 1935-15 components. The green box is MEAD 62B

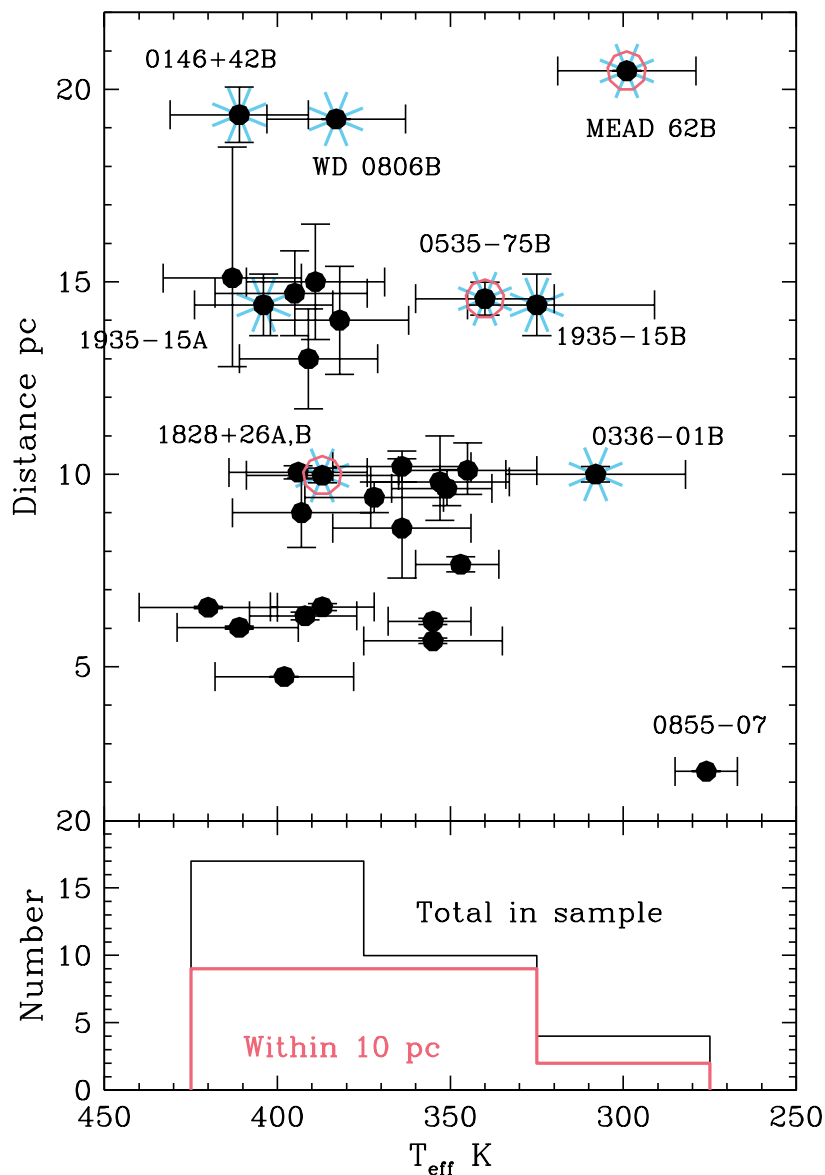


Figure 5. The cold solar neighborhood Y dwarfs from Table 4. Data points with red circles are unconfirmed. Data points with blue asterisks are components of binary systems.

where the age has been constrained to be equal to that of the white dwarf, 4.5 – 10.8 Gyr (Albert et al. 2025a). This constraint on age, combined with our T_{eff} estimate, indicates a range in mass for MEAD 62B of 9 to 12 M_{Jupiter} , if it is indeed a companion to the white dwarf.

The ages of the WISE 0336-01 and WISE 1935-15 systems are not constrained, but I assume that each binary is coeval. Adopting an age range of 0.5 to 10 Gyr for a local dwarf population (e.g. Buder et al. 2019) then the range in masses are: 6 – 28 and 2 – 17 M_{Jupiter} for WISE 0336-01 A and B, and 5 – 25 and 2 – 18 M_{Jupiter} for WISE 1935-15 A and B. The range in mass correlates with the range

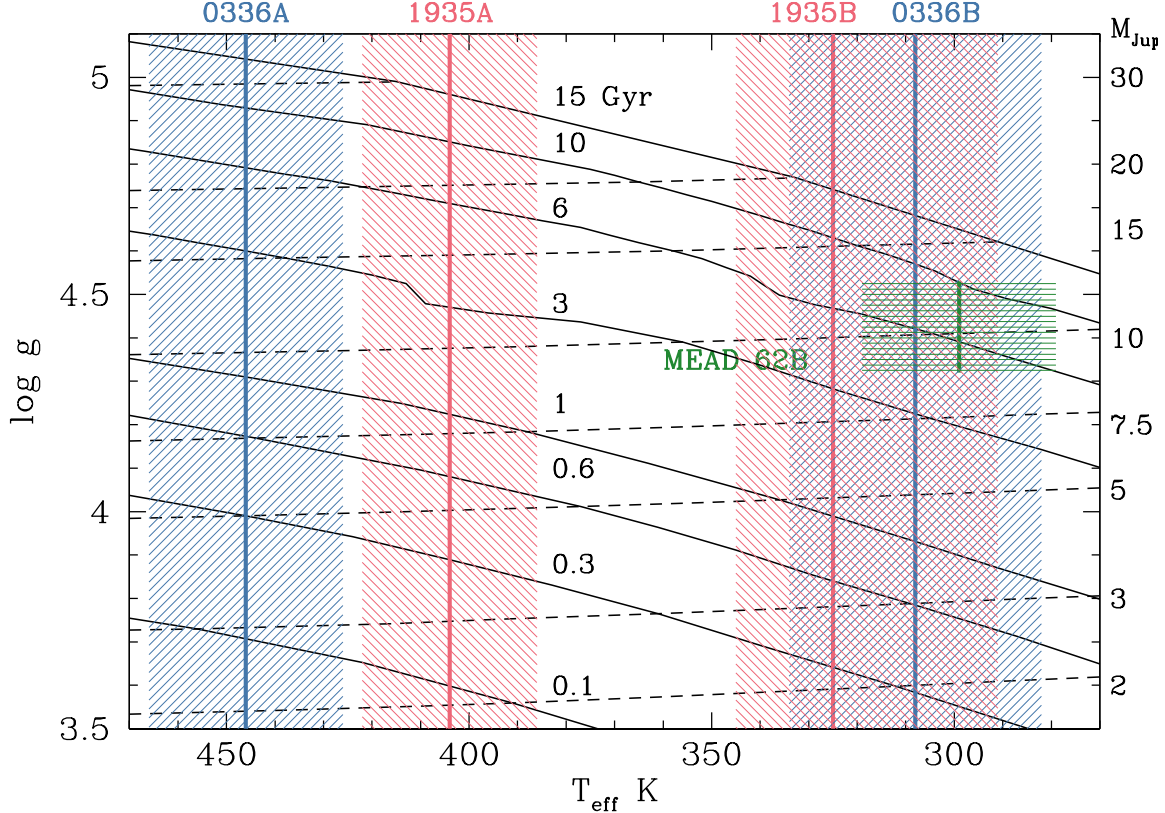


Figure 6. Evolutionary diagram for Y dwarfs from models by Marley et al. (2021). Solid black lines are constant age, with age in Gyr above each line. Dashed lines are iso-mass sequences with mass given on the right axis. Blue vertical line and hashed regions indicate the T_{eff} values and their uncertainties for the WISE 0336-01 binary system. Red lines and regions indicate the same for the WISE 1935-15 binary system. The green line and rectangular region illustrate the T_{eff} and uncertainty for MEAD 62B, restricting the age to be that of the white dwarf primary, 4.5 – 10.8 Gyr (Albert et al. 2025a).

Table 5. Binary Systems with Cold Y Dwarf Secondaries

System	Primary		Secondary		Separation		Reference	
Name	Age (Gyr)	T_{eff} (K)	Mass (M_{Jup})	T_{eff} (K)	Mass (M_{Jup})	mas	au	
WISE 0336-01	0.5 – 10.0	446 ± 20	6 – 28	308 ± 26	2 – 17	84	0.97	Calissendorff et al. (2023)
MEAD 62*	$6.64^{+4.15}_{-2.14}$	5968 ± 124	628 ± 20	299 ± 20	9 – 12	1953	40.0	Albert et al. (2025a)
WISE 1935-15	0.5 – 10.0	404 ± 20	5 – 25	325^{+20}_{-34}	2 – 18	172	2.48	De Furio et al. (2025)

*Also known as 2MASS J09424023-4637176. The primary is a magnetic DA white dwarf (O’Brien et al. 2023); the candidate Y dwarf secondary has not been confirmed to be associated with the white dwarf however the colors and luminosity are consistent with a 299 K dwarf at the distance of the white dwarf.

NOTE—The ages of the Y dwarf binary systems are assumed to be between 0.5 and 10 Gyr, typical of a local population (e.g. Buder et al. 2019). The age of the white dwarf system and the white dwarf temperature is from Albert et al. (2025a). The brown dwarf T_{eff} values are photometric estimates using the relationships presented in this work. Masses for the brown dwarfs are determined using age and T_{eff} and the Marley et al. (2021) evolutionary models. The mass of the white dwarf is from Albert et al. (2025a).

in age, that is, the younger the system the smaller the mass and vice versa (Figure 6). Note that the population synthesis of brown dwarfs within 25 pc by Best et al. (2024) shows that more than 90% of the population is younger than 4 Gyr, implying that the masses of the cold binary components are unlikely to be at the high end of their ranges. For a solar-like age, the component masses are 19 and 9 M_{Jupiter} for WISE 0336-01 A and B, and 17 and 11 M_{Jupiter} for WISE 1935-15 A and B (Figure 6). The properties of the three systems are summarized in Table 5.

6. CONCLUSIONS

A decade after the discovery of WISE 0855-07 (Luhman 2014), three objects have been found which may rival its extremely low temperature and luminosity. Two of these are secondary components of Y dwarf+Y dwarf binary systems: WISE 0336-01B and WISE 1935-15B are in tight configurations with warmer Y dwarfs (Calissendorff et al. 2023; De Furio et al. 2025). The third object, MEAD 62B, needs to be confirmed as a true companion, but it appears to be a cold Y dwarf in a wider configuration with a white dwarf primary (Albert et al. 2025a).

In this work I have determined relationships between mid-infrared colors and T_{eff} , where the T_{eff} values have been constrained by measurements of bolometric luminosity. For very cold Y dwarfs a measurement of luminosity provides tight constraints on T_{eff} (Figure 1). Luminosity-based T_{eff} values have been taken from Beiler et al. (2024) and determined here (Section 2).

Weighted regression fits showed that cubic polynomials reproduced color trends with T_{eff} well, once 3σ outliers were removed. The *rms* of the fits is on average 14 K, however a comparison of T_{eff} values for each color for a larger sample of T and Y dwarfs suggests that the uncertainty floor is ≈ 60 K for 750 K late-T dwarfs, ≈ 40 K for 550 K late-T/early Y dwarfs, and ≈ 20 K for 350 K Y dwarfs.

Six atypical brown dwarfs were excluded from the regression fitting. Two have the spectral signatures of metal-paucity and/or increased gravity (and hence age): WISE J024714.52+372523.5 and WISEA J215949.54-480855.2. Two have the spectral signatures of metal enrichment and/or decreased gravity (and hence age): CWISEP J104756.81+545741.6 and WISE J150115.92-400418.4. WISE J053516.80-750024.9 may be metal-poor and high-gravity, but is better fit as an unresolved binary consisting of 480 K and 340 K Y dwarfs. WISE J043052.92+463331.6 has a peculiar SED which cannot currently be interpreted.

The color: T_{eff} relationships determined here were used to estimate the T_{eff} values for the coldest known Y dwarfs, including the candidate cold Y dwarf secondaries in known or suspected binary systems. I built a sample of 31 objects with $275 \leq T_{\text{eff}} \text{ K} \leq 425$ at distances of about 2 to 20 pc (Figure 5); this assumes that WISE 0535-75 and WISE 1828+26 are unresolved binary systems (Sections 2 and 3), and MEAD 62B is a Y dwarf companion to the white dwarf (Albert et al. 2025a). I find $299 \leq T_{\text{eff}} \leq 325$ for WISE 0336-01B, WISE 1935-15B, and the candidate MEAD 62B, and evolutionary models indicate that their masses are $\sim 10 M_{\text{Jupiter}}$ if the systems are a few Gyrs old (Marley et al. 2021). The sample provides a high priority target list for *JWST* observations, given that it covers the critical regime where water clouds form in the photosphere (Morley et al. 2014).

Cool brown dwarfs are now being found at kpc distances in *JWST* data (e.g. Burgasser et al. 2024; Hainline et al. 2024, 2025; Tu et al. 2025). In the Appendix I give measured and synthesized *JWST* colors for a sample of brown dwarfs, including the extremely metal-poor 500 K object WISEA J153429.75-104303.3, also known as ‘‘The Accident’’ (Kirkpatrick et al. 2021b; Faherty et al. 2025).

These colors will be useful references for deep searches for cold brown dwarfs in *JWST* data, which may probe metal-poor populations in the Milky Way.

The author is grateful to the anonymous referee whose comments greatly improved this manuscript.

APPENDIX

A. *JWST* COLORS FOR IDENTIFYING DISTANT COLD BROWN DWARFS

Recently, distant candidate brown dwarfs have been found in deep searches of *JWST* data (e.g. Burgasser et al. 2024; Hainline et al. 2024, 2025; Tu et al. 2025). In order to classify these objects, synthetic colors calculated by model atmospheres are generally used. In this section I provide *JWST* observational colors for a sample of brown dwarfs which can be used as a reference for the distant population. I use the five filters of the JADES survey (Hainline et al. 2025), which overlap with the filters used by the UNCOVER survey (Burgasser et al. 2024): F115W, F150W, F277W, F410M, and F444W.

The primary data source is the Beiler et al. (2024) sample of T and Y dwarfs with luminosity-based T_{eff} values. Beiler et al. (2024) synthesize F115W, F150W, F277W, F410M, and F444W colors using their low-resolution spectra. I add three objects to this sample: WISE 0855-07, WISEA J153429.75-104303.3 (hereafter WISE 1534-10), and WISE 1828+26. The photometry is synthesized from the NIRSpec spectra published by Luhman et al. (2024) and Faherty et al. (2025), and the spectra obtained for WISE 1828+26 as part of the *JWST* Cycle 1 GTO program 1189, PI: Thomas Roellig. The photometry is given in Table 6.

WISE 1534-10 is of particular interest as it appears to be a cold, extremely metal-poor, halo brown dwarf (Kirkpatrick et al. 2021b; Faherty et al. 2025). Searches for distant brown dwarfs may find metal-poor members of the thick disk and halo (e.g. Imig et al. 2023) and so this object, although highly unusual compared to the local brown dwarf sample, may be relevant for deep searches.

Table 6. New Synthesized *JWST* Photometry, Vega Magnitudes

Name	F115W	F150W	F277W	F410M	F444W
WISE J085510.83-071442.5	25.66	24.00	21.63	14.69	14.08
WISEA J153429.75-104303.3	25.40	22.58	19.70	15.81	15.78
WISE J182831.08+265037.7	23.30	23.12	20.37	14.58	14.45

NOTE—The uncertainty is dominated by the uncertainty in the absolute flux calibration of the *JWST* instruments, which is currently estimated to be 3% or 0.03 magnitudes.

Table 7. *JWST* Colors from [Beiler et al. \(2024\)](#) and This Work

Name	T_{eff}	F277W –	F115W –	F410M –	F115W –
	K	F444W	F150W	F444W	F277W
WISE J024714.52+372523.5	627^{+35}_{-40}	3.93	-0.12	0.05	0.10
WISEP J031325.96+780744.2	560^{+29}_{-31}	4.15	-0.22	0.13	0.46
WISE J035934.06-540154.6	443^{+23}_{-19}	4.70	-0.29	0.12	-0.32
WISE J043052.92+463331.6	495^{+28}_{-23}	4.20	-0.09	0.01	0.70
WISE J053516.80-750024.9	496^{+28*}_{-23}	5.46	-0.02	0.32	2.16
WISE J073444.02-715744.0	466^{+28}_{-23}	4.70	-0.36	0.17	0.73
WISE J082507.35+280548.5	387 ± 15	5.40	-0.70	0.33	2.47
WISE J085510.83-071442.5	276 ± 9	7.55	1.66	0.61	4.03
ULAS J102940.52+093514.6	705^{+39}_{-49}	3.21	-0.16	-0.09	0.20
CWISEP J104756.81+545741.6	395^{+23}_{-21}	4.89	-0.65	0.10	0.24
WISE J120604.38+840110.6	472^{+26}_{-30}	4.34	-0.51	0.05	1.16
SDSSp J134646.45-003150.4	927^{+58}_{-87}	2.54	-0.10	-0.29	0.17
WISE J140518.39+553421.3	392^{+16}_{-15}	5.83	-0.35	0.31	1.30
CWISEP J144606.62-231717.8	351^{+16}_{-13}	5.44	-0.66	0.37	1.65
WISE J150115.92-400418.4	836^{+49}_{-68}	2.70	-0.18	-0.20	-0.03
WISEA J153429.75-104303.3	$502 \pm 6^{**}$	3.92	2.82	0.13	5.70
WISE J154151.65-225024.9	411^{+18}_{-17}	5.24	-0.67	0.34	1.82
SDSSp J162414.37+002915.6	922^{+53}_{-78}	2.80	-0.12	-0.15	0.00
WISE J182831.08+265037.7	$387 \pm 22^{***}$	5.92	0.18	0.13	2.93
WISE J195905.65-333833.5	750^{+42}_{-56}	3.25	-0.16	-0.13	0.19
WISE J205628.91+145953.2	481^{+26}_{-20}	4.86	-0.45	0.14	1.15
WISE J210200.15-442919.5	549^{+29}_{-30}	4.17	-0.23	0.10	0.37
WISEA J215949.54-480855.2	532^{+30}_{-28}	4.55	-0.15	0.06	0.26
WISE J220905.73+271143.9	355^{+13}_{-11}	6.36	...	0.34	...
WISEA J235402.79+024014.1	347^{+13}_{-11}	6.17	-0.48	0.28	1.65

*This Y dwarf may instead be an unresolved binary made up of 480 K and 340 K dwarfs.

** [Faherty et al. \(2025\)](#) determine $T_{\text{eff}} = 502 \pm 6$ by a retrieval analysis.

*** Assuming that the Y dwarf is composed of an identical pair of Y dwarfs.

NOTE—The uncertainty in each color is estimated to be 4% or 0.04 magnitudes, and is dominated by the uncertainty in the absolute flux calibration of the *JWST* instruments.

Table 7 lists the *JWST* colors used in the [Hainline et al. \(2025\)](#) search for distant brown dwarfs, where the data is taken from [Beiler et al. \(2024\)](#) and Table 6. Figure 7 shows these colors in the [Hainline et al. \(2025\)](#) color selection diagram (their Figure 1). The F277W – F444W color increases with decreasing T_{eff} and Figure 7 suggests that Y dwarfs will have $F277W - F444W \gtrsim 4.0$. In F115W – F150W, the cold WISE 0855-07 and very metal-poor high-gravity WISE 1534-10 are significantly redder than the rest of the sample. In F115W – F277W, WISE 1534-10 is almost 5 magnitudes redder than the more metal-rich and likely younger (and therefore lower gravity, see for example Figure 6) brown dwarfs of similar temperature. The F115W – F277W color also turns to

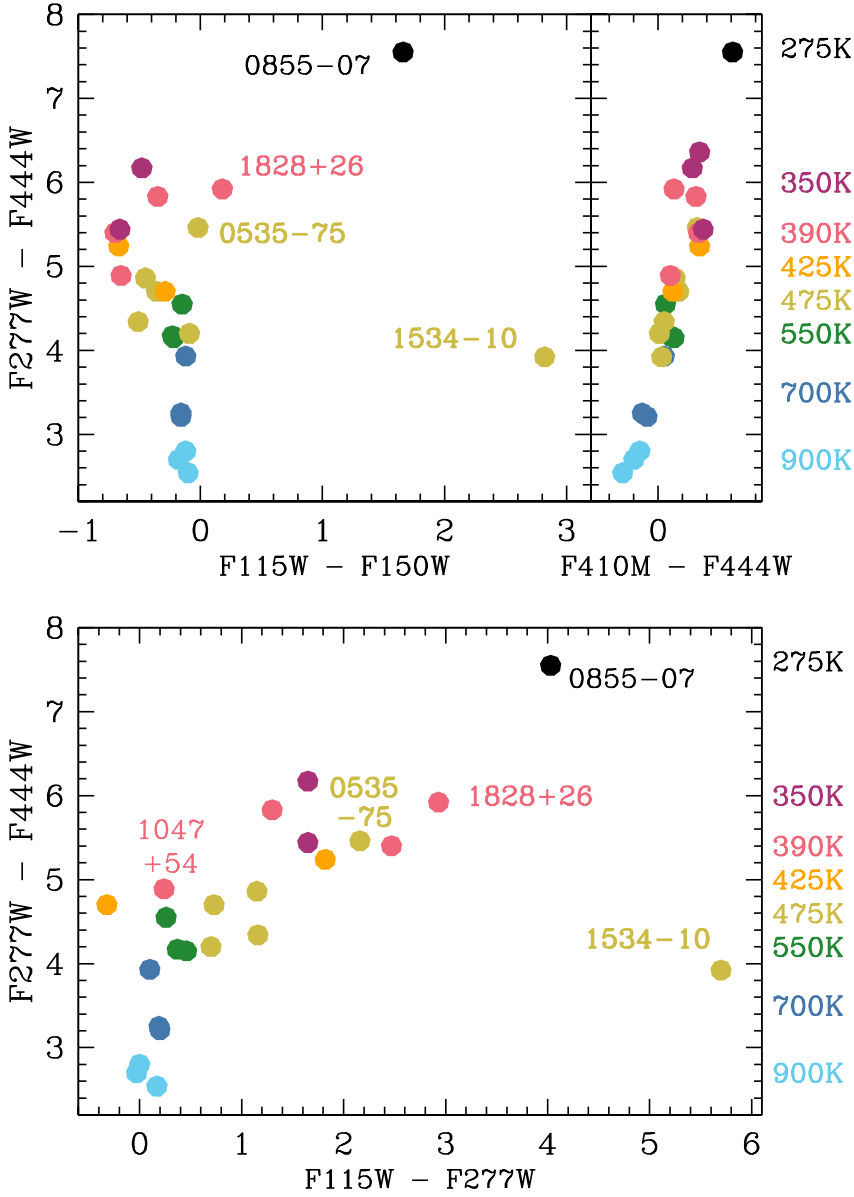


Figure 7. *JWST* colors for the sample in Table 7. Data points are color-coded for T_{eff} as shown in the legends on the right axes. Five brown dwarfs are identified and discussed further in Appendix A.

the red for 400 K and cooler Y dwarfs. As pointed out by Hainline et al. (2025), the $F410M - F444W$ color appears insensitive to metallicity and gravity.

Note that brown dwarfs previously described as unusual have colors somewhat different from objects with similar temperature in Figure 7. WISE 0535-75 is red for its luminosity-based T_{eff} ; it may be an unresolved binary made up of 480 K and 340 K dwarfs, or it may be metal-poor and high-gravity (Section 3.3). WISE 1047+54 is blue, and is very likely to be a young, metal-rich, low-gravity dwarf (Section 3.3). The colors of WISE 1828+26 support the proposed binary nature of this object with $T_{\text{eff}} \approx 387$ K, as opposed to it being a single 462 K brown dwarf (Section 2).

REFERENCES

- Albert, L., Poulsen, S. R., Le Bourdais, É., et al. 2025a, arXiv e-prints, arXiv:2510.12601, doi: [10.48550/arXiv.2510.12601](https://doi.org/10.48550/arXiv.2510.12601)
- Albert, L., Leggett, S. K., Calissendorff, P., et al. 2025b, *AJ*, 169, 163, doi: [10.3847/1538-3881/adadf9](https://doi.org/10.3847/1538-3881/adadf9)
- Baraffe, I., Chabrier, G., Barman, T. S., Allard, F., & Hauschildt, P. H. 2003, *A&A*, 402, 701, doi: [10.1051/0004-6361:20030252](https://doi.org/10.1051/0004-6361:20030252)
- Bardalez Gagliuffi, D. C., Faherty, J. K., Schneider, A. C., et al. 2020, *ApJ*, 895, 145, doi: [10.3847/1538-4357/ab8d25](https://doi.org/10.3847/1538-4357/ab8d25)
- Barrado, D., Mollière, P., Patapis, P., et al. 2023, *Nature*, 624, 263, doi: [10.1038/s41586-023-06813-y](https://doi.org/10.1038/s41586-023-06813-y)
- Beichman, C., Gelino, C. R., Kirkpatrick, J. D., et al. 2013, *ApJ*, 764, 101, doi: [10.1088/0004-637X/764/1/101](https://doi.org/10.1088/0004-637X/764/1/101)
- Beiler, S. A., Cushing, M. C., Kirkpatrick, J. D., et al. 2024, *ApJ*, 973, 107, doi: [10.3847/1538-4357/ad6301](https://doi.org/10.3847/1538-4357/ad6301)
- Best, W. M. J., Liu, M. C., Magnier, E. A., & Dupuy, T. J. 2021, *AJ*, 161, 42, doi: [10.3847/1538-3881/abc893](https://doi.org/10.3847/1538-3881/abc893)
- Best, W. M. J., Sanghi, A., Liu, M. C., Magnier, E. A., & Dupuy, T. J. 2024, *ApJ*, 967, 115, doi: [10.3847/1538-4357/ad39ef](https://doi.org/10.3847/1538-4357/ad39ef)
- Buder, S., Lind, K., Ness, M. K., et al. 2019, *A&A*, 624, A19, doi: [10.1051/0004-6361/201833218](https://doi.org/10.1051/0004-6361/201833218)
- Burgasser, A. J., Geballe, T. R., Leggett, S. K., Kirkpatrick, J. D., & Golimowski, D. A. 2006, *ApJ*, 637, 1067, doi: [10.1086/498563](https://doi.org/10.1086/498563)
- Burgasser, A. J., Bezanson, R., Labbe, I., et al. 2024, *ApJ*, 962, 177, doi: [10.3847/1538-4357/ad206f](https://doi.org/10.3847/1538-4357/ad206f)
- Burrows, A., & Liebert, J. 1993, *Reviews of Modern Physics*, 65, 301, doi: [10.1103/RevModPhys.65.301](https://doi.org/10.1103/RevModPhys.65.301)
- Burrows, A., Marley, M., Hubbard, W. B., et al. 1997, *ApJ*, 491, 856, doi: [10.1086/305002](https://doi.org/10.1086/305002)
- Calissendorff, P., De Furio, M., Meyer, M., et al. 2023, *ApJL*, 947, L30, doi: [10.3847/2041-8213/acc86d](https://doi.org/10.3847/2041-8213/acc86d)
- Cushing, M. C., Kirkpatrick, J. D., Gelino, C. R., et al. 2014, *AJ*, 147, 113, doi: [10.1088/0004-6256/147/5/113](https://doi.org/10.1088/0004-6256/147/5/113)
- . 2011, *ApJ*, 743, 50, doi: [10.1088/0004-637X/743/1/50](https://doi.org/10.1088/0004-637X/743/1/50)
- De Furio, M., Lew, B., Beichman, C., et al. 2023, *ApJ*, 948, 92, doi: [10.3847/1538-4357/acbf1e](https://doi.org/10.3847/1538-4357/acbf1e)
- De Furio, M., Faherty, J. K., Bardalez Gagliuffi, D. C., et al. 2025, *ApJL*, 990, L63, doi: [10.3847/2041-8213/adfee1](https://doi.org/10.3847/2041-8213/adfee1)
- Dupuy, T. J., & Liu, M. C. 2012, *ApJS*, 201, 19, doi: [10.1088/0067-0049/201/2/19](https://doi.org/10.1088/0067-0049/201/2/19)
- Dupuy, T. J., Liu, M. C., & Leggett, S. K. 2015, *ApJ*, 803, 102, doi: [10.1088/0004-637X/803/2/102](https://doi.org/10.1088/0004-637X/803/2/102)
- Faherty, J. K., Meisner, A. M., Burningham, B., et al. 2025, *Nature*, 645, 62, doi: [10.1038/s41586-025-09369-1](https://doi.org/10.1038/s41586-025-09369-1)
- Fontanive, C., Bedin, L. R., Albert, L., & Bardalez Gagliuffi, D. C. 2025, *MNRAS*, 537, 419, doi: [10.1093/mnras/staf032](https://doi.org/10.1093/mnras/staf032)
- Fontanive, C., Bedin, L. R., & Bardalez Gagliuffi, D. C. 2021, *MNRAS*, 501, 911, doi: [10.1093/mnras/staa3732](https://doi.org/10.1093/mnras/staa3732)
- Gaia Collaboration, Brown, A. G. A., Vallenari, A., et al. 2018, *A&A*, 616, A1, doi: [10.1051/0004-6361/201833051](https://doi.org/10.1051/0004-6361/201833051)
- Hainline, K. N., Helton, J. M., Johnson, B. D., et al. 2024, *ApJ*, 964, 66, doi: [10.3847/1538-4357/ad20d1](https://doi.org/10.3847/1538-4357/ad20d1)
- Hainline, K. N., Helton, J. M., Miles, B. E., et al. 2025, arXiv e-prints, arXiv:2510.00111, doi: [10.48550/arXiv.2510.00111](https://doi.org/10.48550/arXiv.2510.00111)
- Imig, J., Price, C., Holtzman, J. A., et al. 2023, *ApJ*, 954, 124, doi: [10.3847/1538-4357/ace9b8](https://doi.org/10.3847/1538-4357/ace9b8)
- Kirkpatrick, J. D., Cushing, M. C., Gelino, C. R., et al. 2013, *ApJ*, 776, 128, doi: [10.1088/0004-637X/776/2/128](https://doi.org/10.1088/0004-637X/776/2/128)
- Kirkpatrick, J. D., Gelino, C. R., Cushing, M. C., et al. 2012, *ApJ*, 753, 156, doi: [10.1088/0004-637X/753/2/156](https://doi.org/10.1088/0004-637X/753/2/156)
- Kirkpatrick, J. D., Martin, E. C., Smart, R. L., et al. 2019, *ApJS*, 240, 19, doi: [10.3847/1538-4365/aaf6af](https://doi.org/10.3847/1538-4365/aaf6af)
- Kirkpatrick, J. D., Gelino, C. R., Faherty, J. K., et al. 2021a, *ApJS*, 253, 7, doi: [10.3847/1538-4365/abd107](https://doi.org/10.3847/1538-4365/abd107)
- Kirkpatrick, J. D., Marocco, F., Caselden, D., et al. 2021b, *ApJL*, 915, L6, doi: [10.3847/2041-8213/ac0437](https://doi.org/10.3847/2041-8213/ac0437)
- Kirkpatrick, J. D., Marocco, F., Gelino, C. R., et al. 2024, *ApJS*, 271, 55, doi: [10.3847/1538-4365/ad24e2](https://doi.org/10.3847/1538-4365/ad24e2)

- Kühnle, H., Patapis, P., Mollière, P., et al. 2024, arXiv e-prints, arXiv:2410.10933, doi: [10.48550/arXiv.2410.10933](https://doi.org/10.48550/arXiv.2410.10933)
- Leggett, S. K., Morley, C. V., Marley, M. S., & Saumon, D. 2015, *ApJ*, 799, 37, doi: [10.1088/0004-637X/799/1/37](https://doi.org/10.1088/0004-637X/799/1/37)
- Leggett, S. K., Morley, C. V., Marley, M. S., et al. 2013, *ApJ*, 763, 130, doi: [10.1088/0004-637X/763/2/130](https://doi.org/10.1088/0004-637X/763/2/130)
- Leggett, S. K., Phillips, M. W., & Tremblin, P. 2025a, *ApJ*, 991, 193, doi: [10.3847/1538-4357/adf21f](https://doi.org/10.3847/1538-4357/adf21f)
- . 2025b, *ApJ*, 995, 132, doi: [10.3847/1538-4357/ae23cd](https://doi.org/10.3847/1538-4357/ae23cd)
- Leggett, S. K., & Tremblin, P. 2024, *Research Notes of the American Astronomical Society*, 8, 13, doi: [10.3847/2515-5172/ad1b61](https://doi.org/10.3847/2515-5172/ad1b61)
- . 2025, *ApJ*, 979, 145, doi: [10.3847/1538-4357/ad8fa6](https://doi.org/10.3847/1538-4357/ad8fa6)
- Leggett, S. K., Tremblin, P., Esplin, T. L., Luhman, K. L., & Morley, C. V. 2017, *ApJ*, 842, 118, doi: [10.3847/1538-4357/aa6fb5](https://doi.org/10.3847/1538-4357/aa6fb5)
- Leggett, S. K., Tremblin, P., Saumon, D., et al. 2016, *ApJ*, 824, 2, doi: [10.3847/0004-637X/824/1/2](https://doi.org/10.3847/0004-637X/824/1/2)
- Leggett, S. K., Dupuy, T. J., Morley, C. V., et al. 2019, *ApJ*, 882, 117, doi: [10.3847/1538-4357/ab3393](https://doi.org/10.3847/1538-4357/ab3393)
- Leggett, S. K., Tremblin, P., Phillips, M. W., et al. 2021, *ApJ*, 918, 11, doi: [10.3847/1538-4357/ac0cfe](https://doi.org/10.3847/1538-4357/ac0cfe)
- Lew, B. W. P., Roellig, T., Batalha, N. E., et al. 2024, *AJ*, 167, 237, doi: [10.3847/1538-3881/ad3425](https://doi.org/10.3847/1538-3881/ad3425)
- Luhman, K. L. 2014, *ApJL*, 786, L18, doi: [10.1088/2041-8205/786/2/L18](https://doi.org/10.1088/2041-8205/786/2/L18)
- Luhman, K. L., Burgasser, A. J., & Bochanski, J. J. 2011, *ApJL*, 730, L9, doi: [10.1088/2041-8205/730/1/L9](https://doi.org/10.1088/2041-8205/730/1/L9)
- Luhman, K. L., & Esplin, T. L. 2016, *AJ*, 152, 78, doi: [10.3847/0004-6256/152/3/78](https://doi.org/10.3847/0004-6256/152/3/78)
- Luhman, K. L., Tremblin, P., Alves de Oliveira, C., et al. 2024, *AJ*, 167, 5, doi: [10.3847/1538-3881/ad0b72](https://doi.org/10.3847/1538-3881/ad0b72)
- Mace, G. N., Kirkpatrick, J. D., Cushing, M. C., et al. 2013, *ApJS*, 205, 6, doi: [10.1088/0067-0049/205/1/6](https://doi.org/10.1088/0067-0049/205/1/6)
- Marley, M. S., Saumon, D., Visscher, C., et al. 2021, *ApJ*, 920, 85, doi: [10.3847/1538-4357/ac141d](https://doi.org/10.3847/1538-4357/ac141d)
- Marocco, F., Caselden, D., Meisner, A. M., et al. 2019, *ApJ*, 881, 17, doi: [10.3847/1538-4357/ab2bf0](https://doi.org/10.3847/1538-4357/ab2bf0)
- Meisner, A. M., Leggett, S. K., Logsdon, S. E., et al. 2023, *AJ*, 166, 57, doi: [10.3847/1538-3881/acdb68](https://doi.org/10.3847/1538-3881/acdb68)
- Meisner, A. M., Caselden, D., Kirkpatrick, J. D., et al. 2020a, *ApJ*, 889, 74, doi: [10.3847/1538-4357/ab6215](https://doi.org/10.3847/1538-4357/ab6215)
- Meisner, A. M., Faherty, J. K., Kirkpatrick, J. D., et al. 2020b, *ApJ*, 899, 123, doi: [10.3847/1538-4357/aba633](https://doi.org/10.3847/1538-4357/aba633)
- Morley, C. V., Marley, M. S., Fortney, J. J., et al. 2014, *ApJ*, 787, 78, doi: [10.1088/0004-637X/787/1/78](https://doi.org/10.1088/0004-637X/787/1/78)
- O'Brien, M. W., Tremblay, P.-E., Gentile Fusillo, N. P., et al. 2023, *MNRAS*, 518, 3055, doi: [10.1093/mnras/stac3303](https://doi.org/10.1093/mnras/stac3303)
- Phillips, M. W., Tremblin, P., Baraffe, I., et al. 2020, *A&A*, 637, A38, doi: [10.1051/0004-6361/201937381](https://doi.org/10.1051/0004-6361/201937381)
- Saumon, D., & Marley, M. S. 2008, *ApJ*, 689, 1327, doi: [10.1086/592734](https://doi.org/10.1086/592734)
- Schneider, A. C., Cushing, M. C., Kirkpatrick, J. D., et al. 2015, *ApJ*, 804, 92, doi: [10.1088/0004-637X/804/2/92](https://doi.org/10.1088/0004-637X/804/2/92)
- Subasavage, J. P., Jao, W.-C., Henry, T. J., et al. 2009, *AJ*, 137, 4547, doi: [10.1088/0004-6256/137/6/4547](https://doi.org/10.1088/0004-6256/137/6/4547)
- Tinney, C. G., Faherty, J. K., Kirkpatrick, J. D., et al. 2012, *ApJ*, 759, 60, doi: [10.1088/0004-637X/759/1/60](https://doi.org/10.1088/0004-637X/759/1/60)
- Tu, Z., Wang, S., Chen, X., & Liu, J. 2025, *ApJS*, 281, 49, doi: [10.3847/1538-4365/ae112e](https://doi.org/10.3847/1538-4365/ae112e)
- Tu, Z., Wang, S., & Liu, J. 2024, *ApJ*, 976, 82, doi: [10.3847/1538-4357/ad815a](https://doi.org/10.3847/1538-4357/ad815a)
- Vasist, M., Mollière, P., Kühnle, H., et al. 2025, *A&A*, 703, A70, doi: [10.1051/0004-6361/202554282](https://doi.org/10.1051/0004-6361/202554282)
- Vrba, F. J., Schneider, A. C., Munn, J. A., et al. 2026, *ApJ*, 999, 24, doi: [10.3847/1538-4357/ae3963](https://doi.org/10.3847/1538-4357/ae3963)